Article:
Forschner, Lukas, Fogang, Lionel T., Gembus, Jan Luca et al. (2026) Characterization of discharge types during cathodic plasma electrolysis. Journal of Physics D: Applied Physics. 115203. ISSN: 0022-3727

https://doi.org/10.1088/1361-6463/ae3b4e

Journal of Physics D:
Applied Physics

Characterization of discharge types during cathodic plasma electrolysis

To cite this article: Lukas Forschner *et al* 2026 *J. Phys. D: Appl. Phys.* **59** 115203

Journal of Physics D: Applied Physics

OPEN ACCESS

RECEIVED
27 August 2025

REVISED
30 November 2025

ACCEPTED FOR PUBLICATION
21 January 2026

PUBLISHED
18 March 2026

PAPER

Characterization of discharge types during cathodic plasma electrolysis

Lukas Forschner[1], Lionel T Fogang[1], Jan-Luca Gembus[2], Nikita Bibinov[2], Lars Schücke[2], Peter Awakowicz[2], Andrew R Gibson[2,3], Timo Jacob[1,*] and Albert K Engstfeld[1,*]

[1] Institute of Electrochemistry, Ulm University, D-89081 Ulm, Germany
[2] Chair of Applied Electrodynamics and Plasma Technology, Ruhr University Bochum, D-44801 Bochum, Germany
[3] York Plasma Institute, School of Physics, Engineering and Technology, University of York, York UK-YO10 5DD, United Kingdom
[*] Authors to whom any correspondence should be addressed.

E-mail: timo.jacob@uni-ulm.de and albert.engstfeld@uni-ulm.de

Keywords: contact glow discharge electrolysis, plasma electrolysis, arc discharge, glow discharge

Supplementary material for this article is available online

Abstract

In-liquid plasma electrolysis refers to the ignition of a plasma in a thin vapor layer surrounding a solid electrode immersed in a liquid electrolyte and its associated processes. Over the last century, this phenomenon has been described under various names and is frequently denoted as contact glow discharge electrolysis. Previous works could show that the plasma might not solely consist of a glow that extends through the entire vapor layer, as the name implies, but consists of multiple filamentary discharges. Building on our previous work on the statistical evaluation of such discharges (Forschner *et al* 2025 *J. Phys. D: Appl. Phys.* **58** 215204), here we study the discharge properties, such as their general appearance, gas temperature, electron density, current density, electron production mechanism, and the discharge voltage, using optical emission spectroscopy, scanning electron microscopy imaging, and electrolyte potential measurements. Our results indicate that the discharges do not solely consist of glow discharges. Instead, the possible co-existence of other discharges, such as arcs and sparks, is discussed.

1. Introduction

Applying a high voltage between two electrodes of different sizes in an electrolyte, a vapor layer may form around the smaller gas-evolving electrode due to ohmic heating and evaporation of the electrolyte surrounding it. Inside the vapor layer, a plasma is ignited, evident by the emission of light which is characteristic of the species present in the plasma [1]. This process was first observed by Fizeau and Foucault in the middle of the 19th century [2]. The first detailed study was performed in 1950 by Kellogg, who called the phenomenon 'aqueous anode effect', in reference to the anode effect in molten salt electrolysis, where, for example, a CO_2-film forms during the oxidation of a graphite electrode [3]. Several years later, Hickling and Ingram denoted the same process 'Contact Glow Discharge Electrolysis' [4, 5]. This name was most likely chosen to distinguish it from 'Glow Discharge Electrolysis', where a plasma is ignited between a liquid electrolyte and a solid electrode located above the liquid, often under reduced pressure [6–9].

Beside the denotation 'Contact Glow Discharge Electrolysis' [10–22], this process has received many other names, such as 'High Voltage Polarization' [1], 'Plasma Driven Solution Electrolysis' [23], 'Glow-Discharge Electrolysis Plasma' [24–27], 'Electrolytic Plasma' [28–30], 'Solution Plasma' [31–33], 'Electrochemical Discharges' [34, 35], or 'Plasma Electrolysis' [23, 36–44]. Most works focused on applications such as chemical synthesis [4, 24, 45], wastewater treatment [18, 46–48], surface modification [36, 42, 49, 50], or nanoparticle formation [16, 51, 52]. More fundamental studies on the nature or type of the plasma are less common. While most terms above use plasma in a very general way, terms such as 'contact glow discharge electrolysis' imply that the vapor layer is filled with a glow discharge

over the entire volume. The wide use of different denotations for this type of discharge in liquids is not only problematic in finding related literature, but also raises a question about the fundamental physical description of the discharge processes.

There are a few works that indicate that the plasma might not consist of a glow discharge only. Some works refer to 'micro-arcs' [39, 40, 53], a term most likely adopted from 'Plasma Electrolytic Oxidation' or 'Micro-arc Oxidation', where a discharge is ignited in channels through an oxide layer on an electrode surface [36, 54, 55]. Other works, mostly related to micro-machining of otherwise difficult-to-machine workpieces, use the term 'spark-assisted chemical engraving', indicating a possible spark-like nature of the discharges [53, 56, 57]. Further studies showed the filamentary nature of the discharges during in-liquid plasma electrolysis [1, 3, 19, 32, 33, 39, 58, 59]. In our recent work (using the terminology 'contact glow discharge electrolysis'), we confirmed the appearance of individual discharges which span from the electrode to the vapor–electrolyte interface, where the transverse diameter is between 0.2 and 0.6 mm. The discharges are dynamic, and the lifetime of a single discharge is up to 100 μs [60]. Due to the ambiguous nature of the discharges, we adopt the notation 'plasma electrolysis' in this work. This work addresses the question of whether the discharges are indeed glow discharges, more fittingly described as (micro-)arcs, or even another type of discharge.

The glow discharge is one of the most studied types of non-thermal discharge, with its electron temperature significantly exceeding the temperature of the ions and gas atoms/molecules [61, 62]. The free electrons are mainly produced by ionization and secondary emission by ion impact on the cold cathode. Glow discharges are often obtained at reduced pressures between two metal electrodes, although discharges at atmospheric pressures and between a metal and a liquid electrolyte have also been investigated, as discussed above [6–9]. They are characterized by voltages of hundreds of V, current densities in the range of μA cm^{-2} to low A cm^{-2}, and electron densities of 10^8–10^{11} cm^{-3} [61, 63, 64]. Increasing the current in a glow discharge first leads to an expansion of the discharge area at a constant voltage and current density. Once the discharge cannot expand further, the discharge voltage increases in the region called abnormal glow, until it drops significantly when an arc is formed [63].

Arc discharges are capable of carrying large currents (with current densities up to MA cm^{-2}) at low voltages (tens of V) [61, 62]. They are typically sustained by thermionic or field emission of electrons, or a combination of the two [65]. The cathode can heat up locally to temperatures of several thousands of K, often leading to erosion of the electrode [61]. Electron densities reach values between 10^{14} and 10^{19} cm^{-3} [62]. Distinguishing between glow and arc discharges is, however, not always simple in the intermediate regime. For example, instabilities in a glow discharge can lead to a constriction, i.e., reduction of the transverse dimension [61]. This phenomenon may lead to a change in the plasma parameters, e.g., an increase in electron density and temperature, as well as erosion of the electrode surface [66]. While recent works discuss the transition between different discharge types, especially glow and arc discharge, discharges in contacts with liquids are typically not considered explicitly [64, 67–71].

A spark is a non-sustained discharge, i.e., it is highly transient in its formation and extinction. The ignition occurs through a streamer mechanism if a certain electric field strength is exceeded (30 kV cm^{-1} in air at ambient conditions) [61, 72]. In terms of plasma parameters, sparks are similar to arc discharges, i.e., they have a high electron density [61, 73, 74], high currents [61, 72] and high temperatures [61, 72]. If the current is sustained, a spark can transform into an arc discharge via the formation of a cathode spot [61, 72]. Since it is difficult to distinguish between a spark and a short-lived arc, in the following, we will remain vague about this distinction, but will elaborate on the difference in the discussion.

Distinguishing between glow and arc-like discharges thus requires insights into the fundamental plasma properties, namely the gas temperature, electron density, current density, discharge voltage, and the electron production mechanism. In plasma electrolysis, inferring these parameters is difficult due to the increased experimental complexity compared to fundamental gas-phase plasma physics studies, i.e., the presence of a (dynamic) plasma–liquid interface. In this work, we provide additional physical insights into the above-mentioned parameters of the discharges during cathodic plasma electrolysis on a Au wire in an alkaline electrolyte, using a combination of techniques. These include optical emission spectroscopy (OES), electrochemical probes for measuring voltage drops in the electrolyte [75], structural characterization of the electrodes by scanning electron microscopy (SEM), and post-plasma liquid-phase analysis by transmission electron microscopy (TEM) imaging and UV/Vis absorption spectroscopy for nanoparticle characterization.

2. Experimental

The spectroscopy experiments were performed at Ruhr University Bochum, while all other experiments were performed at Ulm University. Consequently, the experimental conditions are slightly different, which is detailed below.

2.1. Materials and electrolysis cell

All electrolysis experiments were performed in a rectangular borosilicate glass cell ($20 \times 5 \times 5$ cm) filled with 200 ml of 0.01 M KOH solution as described previously [75]. For UV/Vis emission spectroscopy, a quartz glass cell of the same dimensions was used. For the spectroscopy, the KOH solution was prepared from KOH pellets ($\geqslant$85%, Carl Roth) and deionized water ($\leqslant 700\,\mu S\,cm^{-1}$). For all other experiments, KOH pellets (99.99%) from Sigma-Aldrich and Milli-Q water (18.2 MΩcm, TOC $\leqslant$3 ppb) were used. Before each experiment, the Au wire electrode ($\geqslant$ 99.99%, diameter 0.5 mm, MaTecK) was annealed for 3 min in a propane flame (CAMPINGAZ or MTI). Electrode holders, which can be placed in specific positions along the horizontal axis of the electrolysis cell, were 3D-printed using chemically resistant PVDF from 3Dogg.

2.2. Electrolysis

In all experiments, the voltage was applied between the Au wire working electrode (WE), which was immersed so that 1 cm was in contact with the electrolyte, and a fully immersed stainless steel block counter electrode ($2 \times 2 \times 0.4$ cm). The distance between the two electrodes was 2 cm. The voltage was applied for 300 s in the spectroscopic measurements and 100 s for the measurements of the electrolyte potentials. The plasma ignited after around 80 s. In the spectroscopy experiments, a voltage of 300 V was applied using a Magpuls MP2-30 power supply and recorded using a digital oscilloscope (WaveRunner 8254 2.5 GHz, Teledyne LeCroy). Otherwise, a TDK Lambda GEN600-1.3 power supply was used.

2.3. Optical emission spectroscopy

Optical emission (OE) spectra were recorded using a relatively calibrated, high-resolution spectrometer (ARYELLE Butterfly, LTB Lasertechnik Berlin GmbH). The spectra shown in this work were obtained by averaging five spectra recorded with an acquisition time of 10 s each. The entrance of the spectrometer was connected to a 200 μm quartz fiber with a collimator lens to increase the measured light intensity. The sample was aligned with the spectrometer optic using an LED, focused on the center of the wire electrode.

2.4. Scanning electron microscopy

Scanning electron microscopy (SEM) images were taken with a Quattro SEM from Thermo Fisher Scientific using an accelerating voltage of 20 kV.

2.5. Electrolyte potential mapping

The electrolyte potential can be determined using electrochemical reference electrodes, as illustrated previously in normal high-voltage electrolysis (no plasma) [75]. Two reversible hydrogen electrodes (RHEs) were placed at different positions in the cell, as described previously (including a schematic illustration of the setup) [75]. One RHE was kept at a reference position 10 cm from the closest electrolysis electrode, i.e., for measurements on the WE side the reference RHE is located on the side of the WE, and vice versa. The electrode placement is illustrated in the SI in section S1. Electrolyte potentials between the electrodes were not measured due to the lack of available space between the electrolysis electrodes. For simplicity, in this work all potentials are given versus the RHE on the WE side. At distances larger than 2 cm from the closest electrolysis electrode, the positions are determined accurately by the 3D-printed electrode holders. For distances closer than that, the RHE had to be tilted towards the respective electrode, decreasing the positional accuracy [75]. The working and counter electrode potentials were measured directly versus the RHE at the reference positions. The potential differences were recorded using a National Instruments USB-6009 multifunction DAQ device and an in-house programmed Python software. For high voltages (the potential of the electrodes), a voltage divider was introduced between the electrode and the DAQ device [75].

3. Results

Glow or arc-like discharges can be distinguished by their general appearance, electron density, gas temperature, current density, electron production mechanism, and the discharge voltage. In this section, we

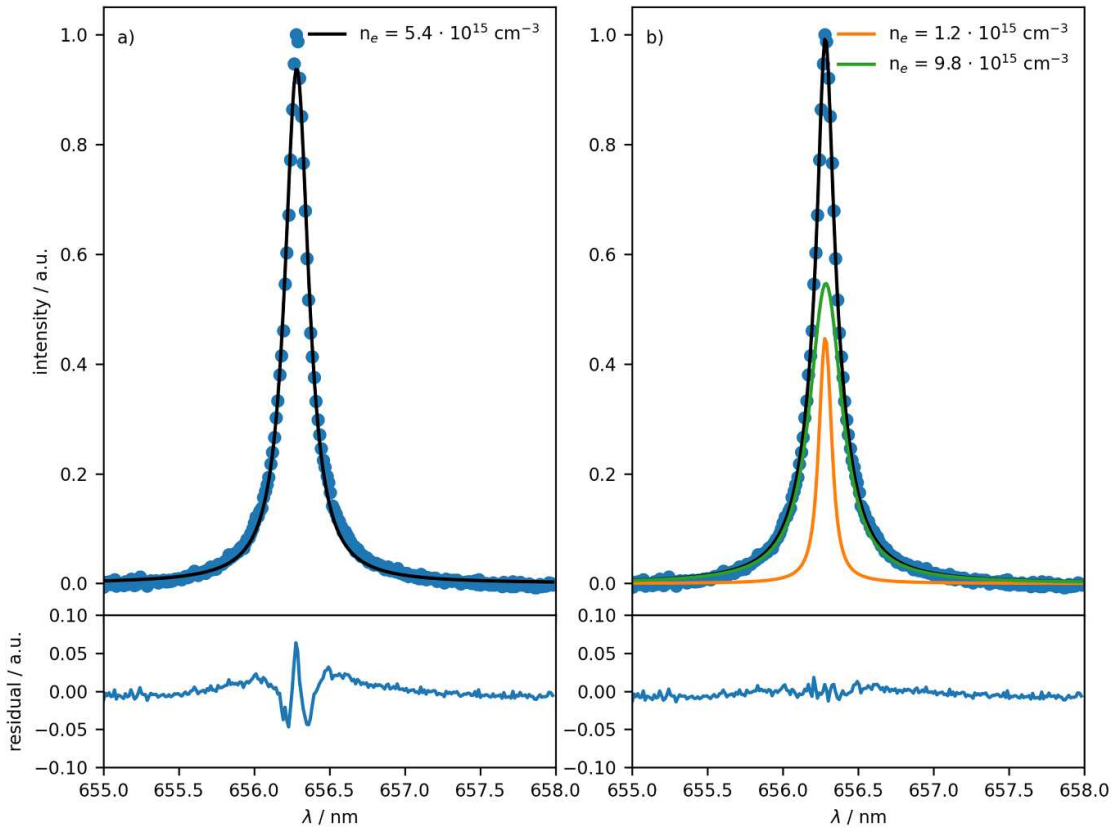

Figure 1. (a) and (b) show the H_α line from an OE spectrum recorded during plasma electrolysis with a Au cathode in 0.01 M KOH at 300 V by blue markers (full spectrum see SI section S2 and S3). In addition, (a) includes a one-density Voigt fit in black and (b) a two-density Voigt fit in black, consisting of the sum of the components in orange and green. The fit residues are provided below the respective plots.

address these properties by individual or combined experiments, providing direct or indirect evidence for either of the discharge types. The results are summarized in the discussion section, including the relation between the individual properties.

3.1. Electron density

The electron density can be inferred from emission lines in OE spectra recorded during plasma electrolysis. The complete OE spectrum can be found in the SI (UV part of the spectrum in figure S2, visible part in figure S3). For the evaluation of the electron density, we focus on the H_α line shown by the blue markers in figures 1(a) and (b). The Stark broadening of this line is calculated with consideration of instrumental, Doppler, and Van-der-Waals broadening. Details on the calculation are given in the SI in section S4. From that, the electron density in the plasma can be estimated if the effect of Stark broadening is sufficiently large, which is typically the case for high electron densities present in arc or spark discharges. Electron densities in a glow discharge are often too small to be estimated in that way [76].

A one-electron-density Voigt fit is shown as a black curve in figure 1(a). Following the conventional method described above and more detailed in the SI in section S4, we obtain an electron density of $5 \times 10^{15}\,\mathrm{cm}^{-3}$. While the fit describes the data reasonably well, the residual shows underfitting in the center and to the sides of the peak, and overfitting in between. This behavior is typical for peaks that are more accurately described by a superposition of more than one profile. Figure 1(b) shows a two-electron-density fit of the same line in black. It is the sum of the profile in orange with an electron density of $(1.2 \pm 0.3) \times 10^{15}\,\mathrm{cm}^{-3}$ and the one in green, giving an electron density of $(9.8 \pm 1.9) \times 10^{15}\,\mathrm{cm}^{-3}$. The residual indicates that this two-density approach fits the data well. As the spectra were recorded over the time frame of several seconds, the result is an average in time and space, including formation and extinction processes of individual discharges. More specifically, the acquisition time is several orders of magnitude longer than the lifetime of the discharges and also the detection region for the OES signal is larger than the separation of individual discharges. Thus, it is not clear whether or not the two distinct electron densities can be attributed to spatially separated regions within individual discharges, different times during the lifetime of individual discharges, or different discharge characteristics

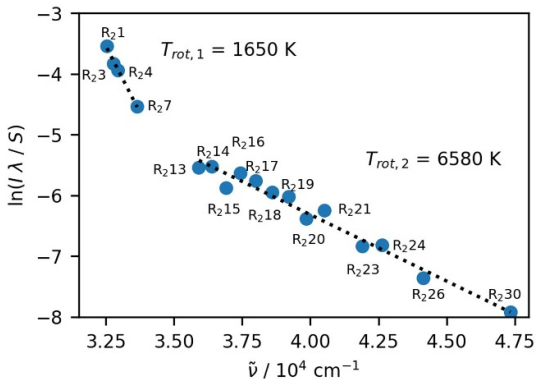

Figure 2. Boltzmann plot of the (0,0) band of the OH $A-X$ transition obtained from OES during plasma electrolysis with a Au cathode in 0.01 M KOH at 300 V. The fits corresponding to two temperatures are indicated as dashed lines. The full OH-region of the spectrum is given in the SI in section S2. The intensities were calculated as described in the text.

occurring in the overall time frame of the measurement. Nevertheless, both electron densities are quite high and have values that strongly indicate the presence of an arc or spark discharge, with typical reported values for gas phase plasmas of 10^{14} to $10^{19}\,\mathrm{cm}^{-3}$ for arcs [62]. Since electron densities cannot be obtained reliably from this method for a glow discharge, this result does not disprove the simultaneous presence of an arc-like and a glow discharge.

3.2. Gas temperature

The gas temperature inside the plasma can be approximated from molecular emission bands observed in OE spectra. This typically involves assuming some equivalence between the rotational temperature of these bands, and the neutral gas temperature. A typical spectrum recorded during the plasma electrolysis for a Au cathode in 0.01 M KOH is shown in the SI (UV part of the spectrum in figure S1, visible part in figure S2). Reliable information is usually obtained from N_2 rotational bands [77–79]. However, no N_2 bands (typically found between 500 and 800 nm for the first positive system and between 300 and 450 nm for the second positive system [78]) are apparent in the OE spectrum, although our cell is not isolated from the ambient air. Instead, we use the emission lines related to the OH-radicals, which show pronounced bands in the spectrum (305–330 nm), clearly resolving the transitions between different rotational levels, where the energy of a transition depends on the rotational level, and the intensity depends, among others, on the rotational temperature. The rotational temperature can be obtained from Boltzmann plots, which for the R_2 branch of the (0,0) band of the OH $A-X$ transition can be obtained from equation (1) [80, 81]:

$$\ln\frac{I\lambda^{v'J'}_{v''J''}}{S_{J'J''}} = \text{const.} - \frac{1}{k_\mathrm{B}T_\mathrm{rot}}E_{v'J'}. \tag{1}$$

Here, I is the intensity of a line, $\lambda^{v'J'}_{v''J''}$ and $S_{J'J''}$ are the wavelength and line strength of a transition, and $E_{v'J'}$ is the energy of the respective excited state with respect to the rotational ground state. The resulting Boltzmann plot is shown in figure 2. The rotational number of the excited state is indicated at each point, i.e., $R_2 1$ is the emission from $J'=1$ to $J''=0$. To fit the data, we assumed two temperatures in different wavelength regions, resulting in a low temperature of 1650 K from lines where J' equals 1, 3, 4, and 7 and a high temperature of 6580 K for $J'\geqslant 13$. Some lines overlap and the maximum can not be inferred unambiguously and are, hence, omitted in the evaluation [80]. This is especially prevalent in the range for $5\leqslant J'\leqslant 12$. Overall, both temperatures are significantly higher than expected for a glow discharge, but not as high as for a typical arc or spark discharge. It should be noted that the determination of the gas temperature using the OH emission suffers from electronic quenching and an overpopulation of states with high J, dependent on the production mechanism of the radicals. Consequently, the intensity distribution can correspond to two or even three different temperatures. This phenomenon has been observed for streamer discharges in vapor bubbles by Bruggeman *et al* [78, 79]. There, the temperature as determined by the N_2 bands agrees with the one from OH only up to around $J=7$. This indicates that for our case, the lower temperature of 1650 K is likely to be more representative of the actual gas temperature.

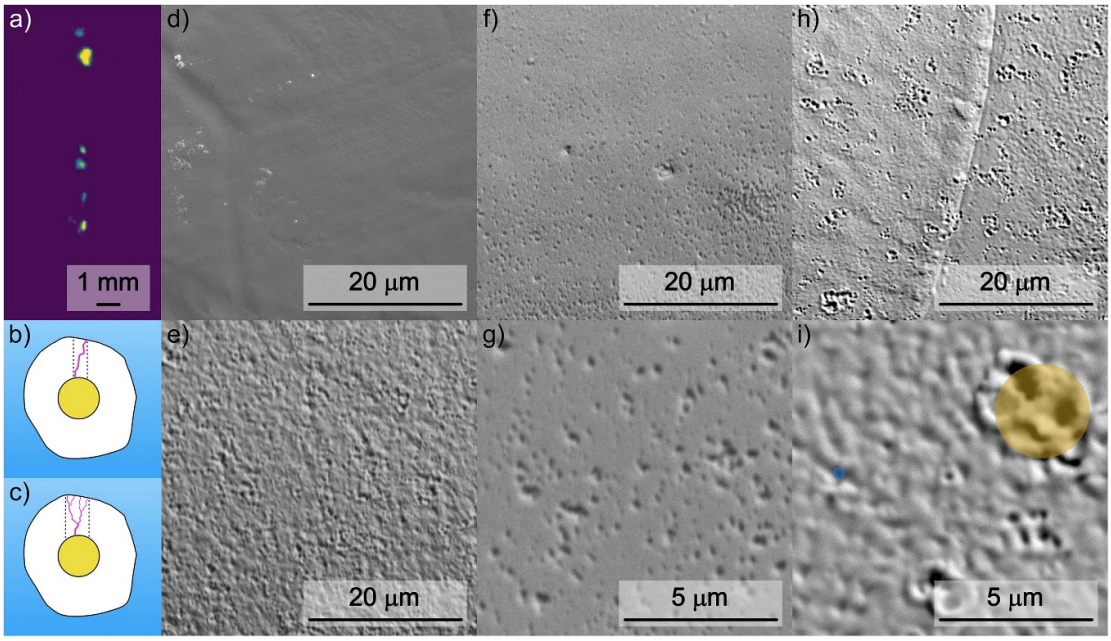

Figure 3. a) High-speed camera image of a Au cathode during plasma electrolysis at 300 V in 0.01 M KOH as described in [60]. (b) Schematic illustration of a discharge meandering through the vapor layer and (c) fanning out from the cathode to the liquid anode, both leading to a higher apparent cross-sectional area. (d) SEM image of an as prepared Au electrode. (e) Au cathode surface after 10 min of plasma electrolysis at 300 V in 0.01 M KOH. (f) and (g) SEM images of the Au electrode surface after normal electrolysis at 300 V in 0.01 M KOH shortly before plasma ignition. (h) and (i) SEM images of the Au electrode shortly after the ignition of plasma electrolysis at 300 V in 0.01 M KOH. One large and one small spot of electrode melting are indicated in orange and blue, respectively.

3.3. Current density

The current density is one of the most reliable properties that allow differentiation between glow and arc discharges. In our experiment, the geometric current density $j = 1.7\,\mathrm{A\,cm^{-2}}$ is simply determined by the measured average current ($I = 0.27\,\mathrm{A}$) divided by the geometric area of the part of the wire electrode that is immersed in the electrolyte ($A_{\mathrm{geo}} = 0.16\,\mathrm{cm^2}$) during plasma electrolysis. This current density is clearly in the range of a glow discharge [61, 63, 64]. As illustrated in the high-speed camera image (without background illumination) of the Au wire electrode during plasma electrolysis in figure 3(a) (see also reference [60]), the plasma consists of individual discharges (bright spots), covering only part of the electrode surface (and the space between the electrode and electrolyte). In fact, based on the statistical evaluation of the size and number of discharges (from high-speed camera images recorded in an interval of 17 μs) present at a given time reported previously [60], we inferred that only 10% of the surface is covered by discharges. Considering that the entire current passes through the discharges, the current density will increase by an order of magnitude, resulting in $j = 17\,\mathrm{A\,cm^{-2}}$, which is already higher than expected for a glow discharge [61, 63, 64]. This simple consideration assumes that the discharges have a perfect cylindrical shape.

From our previous work, we determined from high-speed camera images that the shape of a discharge is predominantly an oblate spheroid, where the minor axis is oriented in the direction of the discharge. This means that the region of impact at the interfaces (plasma–solid and plasma–liquid) might be significantly smaller. Furthermore, the shape determined from individual (or sequences of) images (recorded in an interval of 17 μs) might still not reflect the actual shape or discharge behavior perfectly on a shorter timescale. For example, it is possible that the discharge does not propagate in a straight line from the electrode to the electrolyte but meanders both vertically and horizontally (see figure 3(b), thus appearing wider. Furthermore, the discharge might also fan out, i.e., have a small area close to the cathode and a larger one near the anode, as illustrated schematically in figure 3(c). This means the current density might not be easily determined from images of the discharge, and might also not be constant across the length of the discharge.

One type of arc discharges are arcs with hot cathode spots on a cold cathode [61]. In this case, the cathode spots constitute regions with a high current density, which move rapidly over the surface. This can induce local erosion of the electrode, which in turn can be used to estimate the cathode spot size [61]. To confirm this assumption, we recorded SEM images of the electrode surface slightly before (figures 3(f) and (g), after 75 s of normal electrolysis) and about one second after the ignition of the

plasma (figures 3(h) and (i)). Because the time of plasma ignition varies in the range of about 10 s between experiments, the exact time before the ignition takes place can not be given (but should be in the range of these 10 s). For comparison, an as-prepared electrode surface is shown in figure 3(d), and an electrode surface after a long electrolysis time of 10 min in figure 3(e). It is apparent that normal electrolysis already has an effect on the electrode surface structure, evident from the dark regions in figure 3(f), which could be due to a different composition in these regions or actual holes. We assume the latter is more likely, where the holes might be caused by pitting corrosion. The formation of such structures is discussed in more detail in the SI in section S5.

SEM images of the electrode surface taken shortly after the ignition of the plasma (<1 s) are shown in figures 3(h) and (i). The large-scale image (figure 3(h)) shows local spots with significant differences in brightness, where, in between these spots, the surface also does not seem to be homogeneous (figure 3(i)). Focusing on the dark spots marked in orange and blue in figure 3(i), and considering that the difference in brightness is due to structures with different heights, it seems that electrode material is missing in the center of the spot, which has been transported to the edge, where it is located above the former flat surface. This could be caused by the local melting of the electrode, which is induced by the local impact of single discharges. Note that for longer plasma electrolysis treatment times, the entire electrode has undergone structural changes, as shown in figure 3(e).

Furthermore, considering the hole marked in orange, it is not clear whether that spot is caused by a single discharge, a discharge moving along the wire, or multiple discharges that ignited simultaneously or consecutively in this region. The latter is a likely process, since we observed in our recent works that discharges tend to ignite in the vicinity of agglomerates of discharges [60]. However, considering that these images were taken at less than one second after the plasma ignition, it is expected that the probability of these phenomena is low. Repeating this experiment showed slight differences in the electrode structures obtained before and after the ignition. Nevertheless, the spot sizes where the electrode supposedly melted had a similar size. This is discussed in more detail in the SI in section S5. Further analysis of the electrolyte showed nanoparticle formation, indicating that material is actually removed from the surface and not only transported from the center of the spots to their edges (see SI section S6 for TEM images and size distribution of the nanoparticles as well as a size estimation from the UV/Vis absorption spectrum of the electrolyte). Nevertheless, to estimate the current density through single discharges, we consider the two spots marked in orange and blue as upper and lower bounds of the discharge spot size. Considering a circular geometry, the orange spot has an area of 7.4 μm^2, while the blue spot has an area of 0.13 μm^2. The average total current during plasma electrolysis is 270 mA. However, as there are several discharges present simultaneously, the determination of the current flowing through each cathode spot is quite difficult.

From high-speed camera images we determined the average number of about ten discharges per frame (with an upper bound of 20), similar to the number that can be seen in the high-speed camera image in figure 3(a). We expect additional discharges on the backside of the wire, which is, however, inaccessible to the camera. The number of discharges in that region should be similar or lower compared to these numbers. Assuming a total of 20 simultaneous discharges, and that every discharge carries the same amount of current, we obtain a current density of 182 $kA cm^{-2}$ for the larger cathode spot (orange) and 10.4 $MA cm^{-2}$ for the smaller spot (blue). If the number is smaller than 20, these current densities would even increase. Additionally, one would expect different discharges to carry varying amounts of current. Especially those discharges that cause the melting seen in the SEM images are likely carrying significantly more current than those discharges that do not (yet) induce surface modification.

Assuming that the cathode spots in figure 3(i) are caused by discharges which carry 20% of the total current, one obtains current densities of 730 $kA cm^{-2}$ for the larger cathode spot (orange) and 41.5 $MA cm^{-2}$ for the smaller spot (blue). Note that for this estimation several assumptions were made regarding the cathode spot area and the current of the discharges. However, these currents are clearly in the range of an arc or spark discharge [61, 62, 73, 74], and are significantly larger than those expected for a glow discharge, i.e., in the range of $\mu A cm^{-2}$–$A cm^{-2}$ [61, 63, 64]. Choosing different values for the current, cathode spot area, or number of discharges would still result in current densities in the same range. The presence of a glow discharge in addition to an arc-like discharge can not be excluded. The contribution to the total current would be smaller, though, and no electrode melting would be expected.

3.4. Electron production mechanism

High current densities as the ones obtained above are typically sustained in an arc discharge by thermionic/field emission. Focusing on thermionic emission, where the amount of electrons emitted from the electrode strongly depends on its temperature, one may ask what electrode temperatures are necessary to produce the present current densities. The current density from thermionic emission j_T depends on the

surface temperature T_s as described by the Richardson-Dushman equation [82, 83],

$$j_T = AT_s^2 \exp\left(\frac{-\Phi}{k_B T_s}\right), \tag{2}$$

where A is a constant ($120\,\mathrm{cm^{-2}K^{-2}}$)[84] and $\Phi = 5.22\,\mathrm{eV}$ is the work function [85]. Considering the two limiting cases for the current density for the blue ($41.5\,\mathrm{MA\,cm^{-2}}$) and orange spot ($182\,\mathrm{kA\,cm^{-2}}$) above, electrode temperatures of about 10500 K and 6000 K are expected, respectively. These temperatures are far above the boiling point of Au (3243 K). This is consistent with the spots on the electrode surface in figure 3(i) being ascribed to the melting/evaporation of electrode material. It should be noted that the actual temperature would be lower when considering the effect an electric field, which facilitates the liberation of electrons from the surface. Nevertheless, this result indicates that the presence of an arc discharge is plausible with regard to the electron production mechanism.

3.5. Discharge voltage

Arc and glow discharge can be distinguished by the voltage drop across the discharge, with glow discharges typically showing significantly higher values (hundreds of V) compared to arcs (tens of V). Comparing our system to typical examples from plasma physics, the voltage drop occurs between two driving electrodes, which in our case would be the wire electrode (cathode) and the electrolyte (anode). In a common plasma experiment, the voltage is applied directly to these electrodes. In plasma electrolysis, the voltage is applied between two electrodes immersed in the electrolyte. There, the conductivity of the electrolyte is low, due to the slower ion migration vs. the fast electron migration in the conduction band of a metal. Consequently, the voltage drops in the electrolyte are usually significant for high currents [75]. Thus, the voltage drop (i.e., the potential difference) between the wire and the electrolyte during plasma electrolysis is the voltage applied between the driving electrodes, minus the voltage drop in the electrolyte. To determine the electrolyte potential at the plasma–electrolyte interface, we follow the experimental procedure presented previously [75]. The voltage drop in the electrolyte was measured during high voltage electrolysis (no plasma) with two reference electrodes placed at specific locations in the electrolyte in a cell with well-defined geometry. Thereby, one reversible hydrogen electrode (RHE) is placed at a reference position far away from the electrolysis electrodes. Another RHE is positioned at different locations in the electrolyte, and the voltage between both RHEs is measured. This is illustrated in the SI in section S1. Additionally, the voltage between the electrolysis electrodes and the reference electrode is recorded. For convenience, all potentials are given vs. one reference electrode far away from the driving electrodes on the side of the WE (REF1). Figure 4(a) shows the electrode (WE as squares and counter electrode, CE as triangles) and electrolyte potentials (circles) during normal (blue) and plasma electrolysis (violet) relative to the reference electrode located at −10 cm (REF1). The region between −10 cm and −4 cm is not shown since the potential difference between the RHEs is zero during normal and plasma electrolysis.

The shape of the distance-dependent electrolyte potentials during cathodic normal electrolysis in figure 4(a) (blue) agrees well with that reported in our previous work for anodic normal electrolysis at high voltages [75]. At distances to the WE larger than 0.4 cm, the electrolyte potential distribution is determined by the cell geometry. At positions closer to the WE, the potential followed a logarithmic shape expected from a cylindrically symmetric geometry [5, 86]. The majority of the voltage drops close to the WE due to the small electrolyte cross-section that the current has to pass through in proximity to the thin wire electrode. The voltage drops close to the CE are less pronounced due to the significantly larger size of that electrode, leading to lower current densities at the electrode. In between the electrodes and at a certain distance from the electrodes, the voltage is expected to decrease linearly [75]. Note that values could not be recorded in this region due to the size constraints of positioning our bulky RHE probes.

During plasma electrolysis, the shape of the distance-dependent electrolyte potentials is similar to that during normal high-voltage electrolysis, with two apparent changes. First, the electrolyte potentials close to the electrodes decrease significantly (indicated by black arrows 1) due to the lower current during plasma electrolysis (0.2 A vs. 1.1 A during normal electrolysis). Second, the electrode potentials shift, where the CE potential shifts closer to zero (behaves similarly to the electrolyte potential, arrow 2), but more interestingly, the WE potential shifts to more negative values (arrow 3), indicating a significant additional voltage drop close to the WE with respect to the electrolyte potential.

During normal electrolysis, the difference between the WE potential and any point in the electrolyte is determined by the ohmic voltage drops in the electrolyte. Close to the electrode, and based on our previous study [75], we suggest that the potential distribution should be determined by a cylindrical

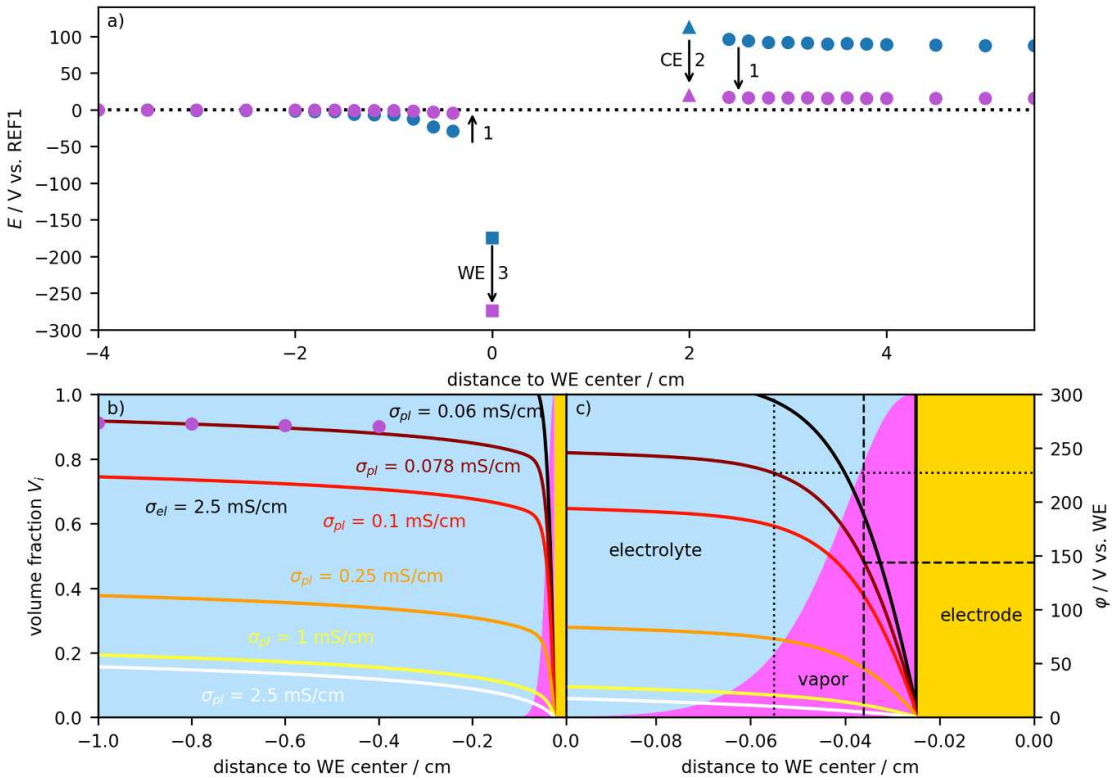

Figure 4. (a) Potentials at the working electrode (WE, square), the counter electrode (CE, triangle), and in the electrolyte (circle) during normal electrolysis (blue) and plasma electrolysis (violet) with a Au wire electrode at 300 V in 0.01 M KOH. The change when the plasma is ignited is indicated by black arrows. (b) and (c) calculated potential distribution, using different conductivities for the plasma, between the working electrode and the closest experimentally determined values for the electrolyte potential. The color of the background illustrates the contributions of the vapor layer and the electrolyte to the total volume in blue and violet, respectively. Note the different *x*-axis scales in each part of the figure.

geometry. Accordingly, in general the difference in potentials φ_i at radii r_i and for constant electrolyte conductivity σ_{el} can be described by [75]

$$\varphi_1 - \varphi_2 = \frac{I}{2\pi\sigma_{\mathrm{el}}L}\ln\frac{r_2}{r_1}, \tag{3}$$

where I is the current and L is the length of the wire. During plasma electrolysis, the region around the WE consists of a vapor layer, the thickness of which fluctuates over time and along the wire. To account for this constraint, we use the vapor layer thickness distribution determined from high-speed camera imaging in a previous work [60], allowing for deriving the volume ratios V_i/V of the respective phase. At distances far from the electrode, the volume fraction of the electrolyte is one, which decreases with decreasing distance to the electrode, where close to the electrode, the volume fraction of the vapor layer with the plasma is one, as illustrated in the colored background of figures 4(b) and (c). Each phase is attributed a conductivity, i.e., σ_{pl} for the plasma phase and σ_{el} for the electrolyte. The latter are weighted according to the volume ratios V_i/V of the respective phases. The change in potential with increasing distance from the electrode is now expressed by the individual volume fractions and respective conductivities, using infinitesimal differences of the potentials and radii:

$$\mathrm{d}\varphi = \frac{I}{2\pi Lr}\mathrm{d}r\left(\frac{V_{\mathrm{pl}}/V(r)}{\sigma_{\mathrm{pl}}} + \frac{V_{\mathrm{el}}/V(r)}{\sigma_{\mathrm{el}}}\right). \tag{4}$$

Furthermore, for this calculation, we simplify the plasma part by assuming that the plasma is homogeneously distributed in the vapor layer and has a single, constant electrical conductivity, contrasting our observation above, where the voltage will likely drop across individual discharges in the vapor layers. A similar assumption was made in the model by Asimakoulas *et al*, who calculated the electric field inside the vapor layer using finite element analysis [87]. The variation of the potential curves was calculated from equation (4) for a fixed electrolyte conductivity of $\sigma_{\mathrm{el}} = 2.5\,\mathrm{mS\,cm^{-1}}$ [88] and varying plasma conductivities (0.06 to 2.5 $\mathrm{mS\,cm^{-1}}$), which are shown as solid curves in figures 4(b) and (c).

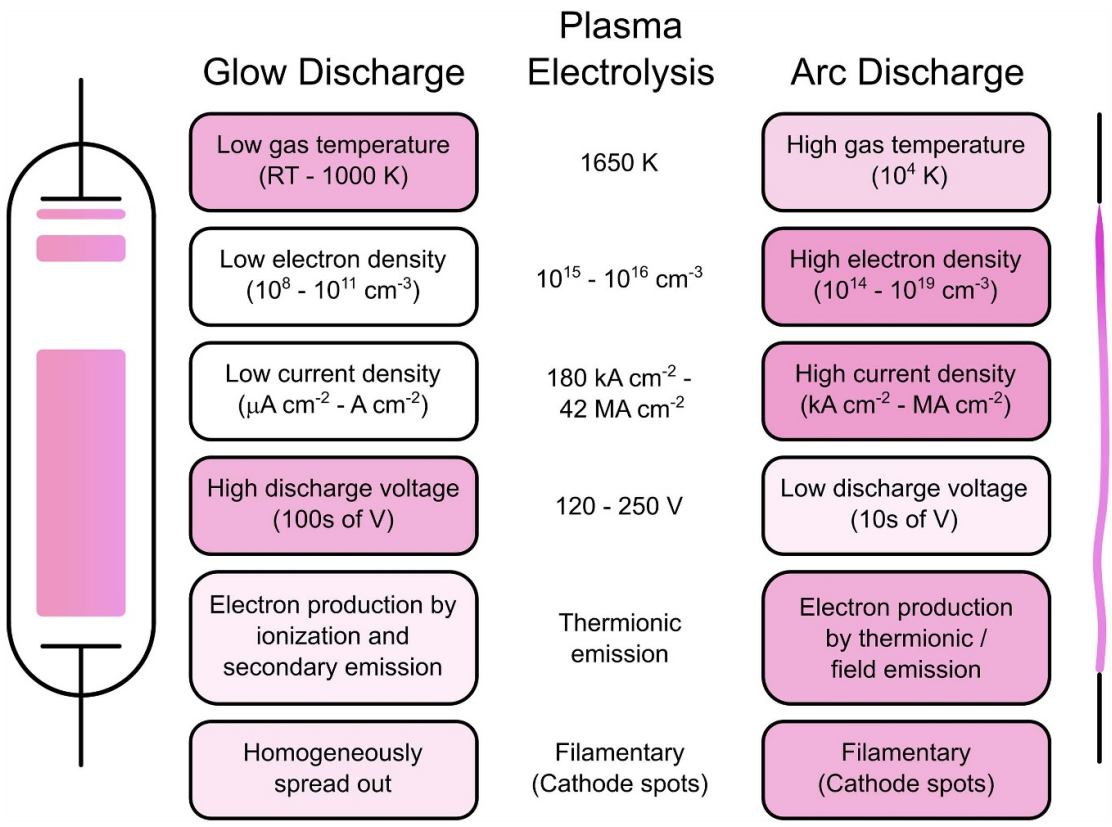

Figure 5. Criteria to distinguish between glow (left) and arc discharge (right). Experimental values are given in the center column. Whether they indicate the presence of a glow or arc discharge is indicated by the opacity of the respective backgrounds.

The best match is obtained with $\sigma_{pl} = 0.078\,\mathrm{mS\,cm^{-1}}$ (dark red curve), which passes through the measured electrolyte potential values (here given with respect to the WE potential) marked by the violet points between -1 and -0.4 cm. For this potential curve, close to the electrode, e.g., at -0.036 cm from the electrode center where 80% of the volume is occupied by vapor, the discharge voltage is approximately 145 V, indicated by the dashed black line. In contrast, at 0.055 cm where only 20% of the volume is occupied by vapor, the discharge voltage is 230 V (dotted black line). These values for the discharge voltage are more typical for a glow discharge, although the real situation is more complicated due to the simultaneous presence of plasma and unionized gas, which would rather correspond to resistances in parallel with a high and low conductivity, respectively. In the case of a glow discharge, the discharge regions could be larger compared to regions with arcs, complicating the assessment even further.

4. Discussion

In our previous work, we showed that the plasma during cathodic plasma electrolysis consists of individual discharges [60]. This raised the question whether the plasma consists of a glow discharge, which is also commonly used in names describing the plasma electrolysis process, such as contact glow discharge electrolysis [18, 19]. While our former work mainly focused on the statistical evaluation of the discharges, to infer their shape, lifetime, or mean velocity, in this work, we performed a set of experiments aiming at gaining a more fundamental understanding of the underlying type of discharge. The results do not clearly provide evidence for a specific type of discharge. Instead, we suggest that the plasma possibly consists of several types of discharges. Focusing on glow and arc discharges, which are suggested to be the most reasonable types of discharges from the visually observed discharge behavior, typical values for the gas temperature, electron density, current density, electron production mechanism, and the discharge voltage are shown in figure 5 along with our experimental results in the center column. We first briefly discuss the experimental results with respect to arc, or arc-like, and glow discharges, and the relation between these results. Second, possible reasons for the concomitant appearance of glow and arc-like discharges are discussed with respect to their ignition and extinction mechanisms.

The result that is most difficult to interpret is the gas temperature, which we estimate from the OH rotational emission spectrum. A Boltzmann plot of the respective lines shows two linear regions. The

lower temperature of about 1650 K is higher than expected for a glow discharge [62, 89], but too low for an arc [62]. The origin of the higher temperature, 6580 K, is unclear. It is possible that the vapor layer contains regions with different types of discharges, e.g., an arc region and a glow region (see below). However, it is likely that the emission from OH radicals simply does not follow a Boltzmann behavior. This is well established and related to the formation processes of OH radicals in the plasma region [78]. Therefore, local thermal equilibrium cannot be guaranteed, and the temperatures are not reliable.

From high-speed camera imaging (see figure 3(a)), it is evident that the plasma does not completely fill the vapor layer, but filamentary discharges can be seen, indicating arcs or arc-like behavior. This interpretation is substantiated by the electron density inferred from OES and the current density through an individual discharge estimated using the local modification of the electrode surface and the number of discharges apparent in high-speed camera imaging. Furthermore, the temperature of the electrode needed to generate the estimated current densities by thermionic emission, as would be expected for an arc discharge, exceeds the boiling point of Au. This is consistent with the formation of holes on the electrode surface, surrounded by deposits from the melt.

The presence of a glow discharge is mainly suggested from visual inspection, but that could be caused by the high frequency and number of arc-like discharges igniting and extinguishing within a second, which the eye or conventional cameras can not differentiate. Experimentally, the glow discharge can be rationalized by the estimated discharge voltage (up to 250 V). If only arc discharges were present, the voltage would be expected to be below 100 V. Note that our estimation of the discharge voltage is based on a simplified model, which does not account for the full complexity of the system. First, we assume that the conductivity within a discharge in the vapor layers is constant and homogeneous. In reality, however, the voltage drop mostly occurs in the sheath regions (close to the electrodes), while in the bulk of the plasma, the electric field is low and the potential is almost constant. This would also mean that the discharge voltage is independent of the size of the discharge gap (distance between the electrode and the electrolyte). Also, if there are different discharges present simultaneously, they would have different potential distributions. Nevertheless, our results provide a reasonable estimate of the mean discharge voltage. Note that while our discharge voltage is quite high and thus hints at the presence of a glow discharge, other examples of plasma electrolysis suggest much lower values. For example, Kellogg observed plasma electrolysis in 0.5 M H_2SO_4 at a Pt wire anode by applying a total voltage of 60 V. Hence, the discharge voltage must be lower, considering the voltage drop in the electrolyte, and a glow discharge seems unlikely in this case.

It is also possible that no sustained discharges are formed, but sparks are initiated in the vapor layer. The electric field strength necessary for breakdown of air in ambient conditions is 30 kV cm^{-1}. For a vapor layer thickness of 0.1 mm, which is on the lower end of the vapor layer thickness distribution [60], the resulting voltage is 300 V. While this voltage is higher than the discharge voltage determined using the electrolyte potentials (between 120 and 250 V), it is reasonably close to consider the presence of sparks. While sparks have similar properties to arcs, i.e., a high electron density, high currents, and high gas temperatures, they are not sustained. While there is continuous emission during plasma electrolysis, it stems from individual discharges that form and disappear on a frequent basis. If the current through a spark is maintained, the spark can transform into an arc discharge [61, 72]. However, arc discharges are typically not stable on electrodes of low melting point, such as the Au used in this work. Thus, it is possible that a spark is ignited first, which then transforms into an arc until the electrode quickly melts/evaporates, providing a natural end to the discharge, which will be discussed further below.

Apart from glow, arc-like or spark-like discharges, other forms of discharges might explain some of the more ambiguous results from this work. For example, inhomogeneities in a glow discharge may lead to a constriction, i.e., reduction of the cross section of the discharge. This can, in turn, affect the plasma parameters, such as the electron density or current density [61]. However, constricted glow discharges are not expected to show lines of the electrode material in the emission spectrum [66], which, for our case, are clearly visible (see section S2 in the SI). Thus, we omit a detailed consideration of such a discharge type.

Following, we rationalize the presence of different types of discharges, describing the possible ignition and extinction process for a single discharge. Plasma electrolysis occurs once a stable vapor layer forms around the plasma electrode. At this point, the electrode is static, but the vapor–electrolyte interface is still rather dynamic. The electrode is possibly still rather cold, as the contact with the electrolyte prior to the ignition constantly cools it. Nevertheless, the large potential difference between the electrode and the electrolyte can be sufficient to locally ignite a glow discharge in the vapor layer. Next, the voltage might increase along with the current density, leading to an abnormal glow, which can, however, not be inferred directly from our experiments. Concomitantly, the cathode temperature increases due to the impact of positive ions until an arc-like discharge appears. This should lead to a decrease

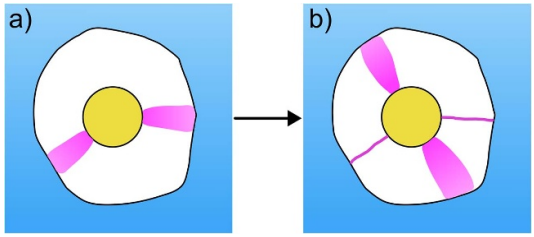

Figure 6. Scheme depicting the evolution of discharges from (a) glow to (b) a simultaneous presence of glow and arc discharges. Glow discharges are illustrated as the wider area discharges and arcs as thin lines.

in discharge voltage [64]. Due to the local restructuring of the electrode depicted by SEM imaging, we assume that the glow has little effect on major electrode restructuring, and that the holes observed on the electrode are mainly caused by the other types of discharges. The arc is then sustained by thermionic emission, potentially supported by the electric field, as described above. However, in our previous work, we could show that the individual discharges have a limited lifetime. We assume that during the arcing process, the electrode surface locally heats further on the cathode spot of the arc. Consequently, the heating will lead to local boiling of the surface, and when this process gets too strong, along with possible spontaneous release of electrode material, the discharge extinguishes. Finally, considering that we observe spatially separated discharges in the high-speed camera images, it is likely that new glow discharges are ignited on the electrode while other discharge types are still present elsewhere on the surface. This is illustrated in figure 6, where in figure 6(a) two glow discharges are present, which develop, in this simple representation, into arcs in figure 6(b), along with the ignition of two new glow discharges. Consequently, the voltage across the vapor layer would then be determined by the glow discharges, although the exact potential distribution for the individual discharges would be complex. Overall, it may seem counterintuitive to simultaneously have discharges with highly different discharge voltages from a plasma physical point of view. Using metals as electrodes, constant electrode potentials are expected. In contrast, when one electrode is an electrolyte, which has a significantly lower conductivity, it is conceivable to have a glow and an arc discharge in parallel, connecting different points at the electrolyte–plasma interface to the metal electrode. The difference in discharge voltage would then appear as an ohmic voltage drop between the two electrolyte locations. Also, note that in a previous work, we noticed that new discharges ignite preferentially above groups of established discharges. This is likely related to species originating from the extinguished discharge, which move due to buoyancy upwards along the wire, eventually facilitating the ignition of new discharges [60].

In total, we related the possible types of plasma during plasma electrolysis to values inferred from typical gas-phase plasma experiments. Considering that we find values which can be related clearly to different types of plasmas, illustrates the complexity of the nature of plasmas in plasma electrolysis. This observation is possibly not surprising, given the presence of a dynamic liquid anode (the electrolyte). Thus, deviations from idealized discharges are expected, and our results do not necessarily reflect the properties of discharges known from their plasma-physical fundamentals. To gain more fundamental insights into the possible temporal changes of individual discharges, a more refined model system and diagnostics other than those presented in this work will be required, especially approaches with higher temporal resolution. Specifically, solutions must be found to reduce the dynamics of the vapor layer. Due to the varying local lateral extent of the vapor layer, care must be taken when comparing these results to theoretical models, where fixed distances between the electrodes are usually assumed. Nevertheless, the statistical results from our previous work and the data from this work might help in gaining more fundamental insights from a theoretical perspective.

5. Conclusion

In this work, we studied the properties of the plasma in cathodic in-liquid plasma electrolysis. To determine the type of discharge present, we combined OES, SEM, and electrochemical measurement of the electrolyte potentials. By considering the discharge itself as well as its interaction with the solid electrode and the liquid electrolyte, we derived a consistent explanation for the temporal evolution of single discharges. The following aspects of the discharges were investigated:

- The electron density in the discharge was calculated using the Stark broadening of the H_α line. This yielded two electron densities of 1.2×10^{15} and $9.8 \times 10^{15}\,cm^{-3}$. While we can make no conclusive statement about the origin of the two electron densities, both values indicate the presence of an arc or spark discharge.
- A Boltzmann-plot of the OH radical emission gave a two-temperature distribution with temperatures of 1650 and 6580 K. While the higher of these two temperatures is likely caused by the non-equilibrium population mechanisms of the higher OH rotational levels, even the lower temperature, which is expected to be more representative of the gas temperature, is higher than expected for a glow discharge. Still, the temperature determination by the OH emission should be viewed with caution as discussed above.
- High-speed camera images of the electrode indicate a filamentary nature of the discharge. The size of the discharge as it appears in the camera image is most likely larger than the cross-sectional area of the discharge due to a meandering or fanning out of the discharge on its path through the vapor layer. On the cathode, the current is concentrated on spots with a size between 0.13 and 7.4 μm^2 as determined from spots of molten electrode material in SEM images.
- Using the cathode spot sizes obtained from the SEM images, we estimated the current density at the cathode spot to be in the range of $180\,kA cm^{-2}$ to $42\,MA cm^{-2}$, clearly indicating an arc discharge.
- To generate the current densities above by thermionic emission, electrode temperatures between 6000 and 10500 K are necessary. These temperatures exceed the boiling point of the Au electrode, which is consistent with the local melting observed on the electrode surface, as well as the presence of Au nanoparticles in the electrolyte.
- The electrolyte potentials were measured electrochemically and extrapolated to the vapor–electrolyte interface. The discharge voltage was determined to be between 120 and 250 V, dependent on the thickness of the vapor layer at the respective position. This indicates the presence of a glow discharge.

Overall, our results clearly indicate the presence of arc- or spark-like discharges during plasma electrolysis. It is, however, possible that the high discharge voltage is caused by the presence of glow discharges. Over time, the electrode heats up until thermionic emission can produce the current densities for an arc to occur. Alternatively, sparks are ignited directly without prior presence of other discharge types. The discharges are likely extinguished with the melting and evaporation of the electrode material at the cathode spot. In conclusion, we recommend to forgo the use of 'Contact Glow Discharge Electrolysis' when describing plasma electrolysis to avoid mistaking the plasma for a classical glow discharge.

Acknowledgement

The authors gratefully acknowledge support from the DFG (German research foundation) through the collaborative research center CRC1316 (Project 327886311, B12 and B5). The authors also thank the Central Facility for Electron Microscopy of Ulm University, particularly Jana Apolloni for the preparation of TEM samples as well as Reinhard Weih and Dr. Clarissa Read for instructing the TEM imaging.

Data availability statement

The data that support the findings of this study are openly available at the following URL/DOI: https://zenodo.org/records/16794625.

Supporting information available at https://doi.org/10.1088/1361-6463/ae3b4e/data1.

CRediT

L Forschner: Conceptualization, Formal Analysis, Investigation, Validation, Visualization, Writing—Original Draft Preparation. **L Fogang**: Investigation, Writing—Review & Editing. **N Bibinov**: Writing—Review & Editing. **J-L Gembus**: Investigation, Writing—Review & Editing. **L Schücke**: Supervision, Writing—Review & Editing. **P Awakowicz**: Funding Acquisition, Resources, Supervision, Writing—Review & Editing. **A R Gibson**: Funding Acquisition, Resources, Supervision, Writing—Review & Editing. **T Jacob**: Funding Acquisition, Resources, Supervision, Writing—Review & Editing. **A K Engstfeld**: Funding Acquisition, Conceptualization, Supervision, Writing—Review & Editing

ORCID iDs

Lukas Forschner 0000-0002-1551-5045
Lionel T Fogang 0000-0002-7357-908X
Jan-Luca Gembus 0009-0002-1263-9218
Lars Schücke 0000-0002-7991-853X
Peter Awakowicz 0000-0002-8630-9900
Andrew R Gibson 0000-0002-1082-4359
Timo Jacob 0000-0001-7777-2306
Albert K Engstfeld 0000-0002-9686-3948

References

[1] Azumi K, Mizuno T, Akimoto T and Ohmori T 1999 Light emission from Pt during high-voltage cathodic polarization *J. Electrochem. Soc.* **146** 3374–7
[2] Fizeau H and Foucault L 1844 Recherches sur l'intensite de la lumiere emise par le charbon dans l'experience de Davy *Ann. Chim. Phys.* **11** 370–84
[3] Kellogg H H 1950 Anode effect in aqueos electrolysis *J. Electrochem. Soc.* **97** 133–42
[4] Hickling A and Newns G R 1961 The contact glow-discharge electrolysis of liquid ammonia *J. Chem. Soc.* 5186–91
[5] Hickling A and Ingram M D 1964 Contact glow-discharge electrolysis *Trans. Faraday Soc.* **60** 783–93
[6] Klemenc A 1931 Über glimmlichtelektrolyse: in gemeinschaft mit H. F. Hohn *Ztschr. Elektrochem.* **37** 742–5
[7] Davies R A and Hickling A 1952 Glow-discharge electrolysis. Part I. the anodic formation of hydrogen peroxide in inert electrolytes *J. Chem. Soc.* 3595–602
[8] Denaro A R and Hickling A 1958 Glow-discharge electrolysis in aqueous solutions *J. Electrochem. Soc.* **105** 265–70
[9] Hickling A and Ingram M D 1964 Glow-discharge electrolysis *J. Electroanal. Chem.* **8** 56–81
[10] Sengupta S K , Singh O P 1991 Contact glow discharge electrolysis: a study of its onset and location *J. Electroanal. Chem.* **301** 189–97
[11] Gao J, Wang A, Fu Y, Wu J, Ma D, Guo X, Li Y and Yang W 2008 Analysis of energetic species caused by contact glow discharge electrolysis in aqueous solution *Plasma Sci. Technol.* **10** 30–38
[12] Gangal U, Srivastava M and Gupta S K S 2009 Mechanism of the breakdown of normal electrolysis and the transition to contact glow discharge electrolysis *J. Electrochem. Soc.* **156** F131–6
[13] Jin X-L, Wang X, Zhang H-M, Xia Q, Wei D-B and Yue J-J 2010 Influence of solution conductivity on contact glow discharge electrolysis *Plasma Chem. Plasma Process.* **30** 429–36
[14] Jin X, Wang X, Yue J, Cai Y and Zhang H 2010 The effect of electrolyte constituents on contact glow discharge electrolysis *Electrochim. Acta* **56** 925–8
[15] Liu Y, Sun B, Wang L and Wang D 2012 Characteristics of light emission and radicals formed by contact glow discharge electrolysis of an aqueous solution *Plasma Chem. Plasma Process.* **32** 359–68
[16] Allagui A, Baranova E A and Wüthrich R 2013 Synthesis of Ni and Pt nanomaterials by cathodic contact glow discharge electrolysis in acidic and alkaline media *Electrochim. Acta* **93** 137–42
[17] Allagui A, Said Z, Abdelkareem M A, Elwakil A S, Yang M and Alawadhi H 2017 DC and AC performance of graphite films supercapacitors prepared by contact glow discharge electrolysis *J. Electrochem. Soc.* **164** A2539–46
[18] Sengupta S K 2017 Contact glow discharge electrolysis: a novel tool for manifold applications *Plasma Chem. Plasma Process.* **37** 897–945
[19] Yerokhin A, Mukaeva V R, Parfenov E V, Laugel N and Matthews A 2019 Charge transfer mechanisms underlying contact glow discharge electrolysis *Electrochim. Acta* **312** 441–56
[20] Alteri G B, Bonomo M, Decker F and Dini D 2020 Contact glow discharge electrolysis: effect of electrolyte conductivity on discharge voltage *Catalysts* **10** 1104
[21] Artmann E, Menezes P V, Forschner L, Elnagar M M, Kibler L A, Jacob T and Engstfeld A K 2021 Structural evolution of Pt, Au and Cu anodes by electrolysis up to contact glow discharge electrolysis in alkaline electrolytes *ChemPhysChem* **22** 2429–41
[22] Artmann E, Forschner L, Jacob T and Engstfeld A K 2022 Using auxiliary electrochemical working electrodes as probe during contact glow discharge electrolysis: a proof of concept study *J. Vac. Sci. Technol. A* **40** 053005
[23] Bespalko S and Mizeracyk J 2022 Overview of the hydrogen production by plasma-driven solution electrolysis *Energies* **15** 7508
[24] Gao J, Li X, Lu Q, Li Y, Ma D and Yang W 2012 Synthesis and characterization of poly(methyl methacrylate-butyl acrylate) by using glow-discharge electrolysis plasma *Polym. Bull.* **68** 37–51
[25] Yu J, Yang G, Li Y, Yang W, Gao J and Lu Q 2013 Synthesis, characterization and swelling behaviors of acrylic acid/carboxymethyl cellulose superabsorbent hydrogel by glow-discharge electrolysis plasma *Polym. Eng. Sci.* **54** 2310–20
[26] Ren J, Yao M, Yang W, Li Y and Gao J 2014 Recent progress in the application of glow-discharge electrolysis plasma *Cent. Eur. J. Chem.* **12** 1213–21
[27] Yu J, Wang B, Lu Q, Xiao L, Ma X, Feng Y and Qian Y 2022 Fabrication of Fe_3O_4 nanoparticles by using cathode glow discharge electrolysis plasma and its electrochemical properties *Electrochim. Acta* **427** 140843
[28] Slovetskii D I and Terent'ev S D 2003 Parameters of an electric discharge in electrolytes and physicochemical processes in an electrolyte plasma *High Energy Chem.* **37** 310–6
[29] Parfenov E V, Farrakhov F G, Mukaeva V R, Gusarov A V, Nevyantseva R R and Yerokhin A 2016 Electric field effect on surface layer removal during electrolytic plasma polishing *Suf. Coat. Technol.* **307** 1329–40
[30] Shadrin S Y, Belkin P N, Tambovskiy I V and Kusmanov S A 2020 Physical features of anodic plasma electrolytic carburising of low-carbon steels *Plasma Chem. Plasma Process.* **40** 549–70
[31] Saito G, Hosokai S, Tsubota M and Akiyama T 2011 Nickel nanoparticles formation from solution plasma using edge-shielded electrode *J. Phys.: Conf. Ser.* **31** 719–28
[32] Saito G, Nakasugi Y and Akiyama T 2014 Excitation temperature of a solution plasma during nanoparticle synthesis *J. Appl. Phys.* **116** 083301

[33] Saito G, Nakasugi Y and Akiyama T 2014 High-speed camera observation of solution plasma during nanoparticle formation *Appl. Phys. Lett.* **104** 083104
[34] Allagui A and Wüthrich R 2009 Gas film formation time and gas film life time during electrochemical discharge phenomenon *Electrochim. Acta* **54** 5336–43
[35] Wüthrich R and Allagui A 2010 Building micro and nanosystems with electrochemical discharges *Electrochim. Acta* **55** 8189–96
[36] Yerokhin A L, Nie X, Matthews A and Dowey S J 1999 Plasma electrolysis for surface engineering *Surf. Coat. Technol.* **122** 73–93
[37] Toriyabe Y, Watanabe S, Yatsu S, Shibayama T and Mizuno T 2007 Controlled formation of metallic nanoballs during plasma electrolysis *Appl. Phys. Lett.* **91** 041501
[38] Zhang Z, Dubey M, Galipeau D, Fan Q H, Hoefelmeyer J D and Al-Qaradawi I Y 2013 Activation of nickel foam through in-liquid plasma-induced phosphorus incorporation for efficient quasi-industrial water oxidation and selective oxygenation of organics *Creating Textured Surfaces Using Plasma Electrolysis* **3** 255–8
[39] Stojadinović S, Jovović J, Tadić N, Vasilić R and Šišović N M 2015 The characterization of cathodic plasma electrolysis of tungsten by means of optical emission spectroscopy techniques *Europhys. Lett.* **110** 48004
[40] Jovović J, Stojadinović S, Tadić N, Vasilić R and Šišović N M 2016 The study of micro-arc discharges during cathodic plasma electrolysis of refractory metals using the spectral line shape of Na I lines *Europhys. Lett.* **113** 68001
[41] Sukreni T, Saksono N and Bismo S 2018 Effect of anode depth and conductivity of electrolyte solution on energy consumption in plasma electrolysis *IOP Conf. Ser.: Earth Environ. Sci.* **105** 012009
[42] Zheng B, Wang K, Shrestha M, Schuelke T and Fan Q H 2019 Understanding the chemical reactions in cathodic plasma electrolysis *Plasma Sources Sci. Technol.* **28** 085016
[43] Menezes P V, Elnagar M M, Al-Shakran M, Eckl M J, Menezes P W, Kibler L A and Jacob T 2022 In-liquid plasma for surface engineering of Cu electrodes with incorporated SiO2 nanoparticles: from micro to Nano *Adv. Fuct. Mater.* **32** 2107058
[44] Yang H, Menezes P V, Dai G, Vijaykumar G, Chen Z, Al-Shakran M, Jacob T, Driess M and Menezes P M 2023 Activation of nickel foam through in-liquid plasma-induced phosphorus incorporation for efficient quasi-industrial water oxidation and selective oxygenation of organics *Appl. Catal. B: Environ.* **324** 122249
[45] Harada K and Iwasaki T 1974 Syntheses of amino acids from aliphatic carboxylic acid by glow discharge electrolysis *Nature* **250** 426–8
[46] Malik M A, Ghaffar A and Malik S A 2001 Water purification by electrical discharges *Plasma Sources Sci. and Technol.* **10** 82–91
[47] Wang X, Zhou M and Jin X 2012 Application of glow discharge plasma for wastewater treatment *Electrochim. Acta* **83** 501–12
[48] Horikoshi S and Serpone N 2017 In-liquid plasma: a novel tool in the fabrication of nanomaterials and in the treatment of wastewaters *RCS Adv.* **7** 47196–218
[49] Paulmier T, Bell J M and Fredericks P M 2007 Development of a novel cathodic plasma/electrolytic deposition technique part 1: production of titanium dioxide coatings *Surf. Coat. Technol.* **201** 8761–70
[50] Artmann E, Forschner L, Schüttler K, Al-Shakran M, Jacob T and Engstfeld A K 2022 Nanoporous Au formation on Au substrates via high voltage electrolysis *ChemPhysChem* **24** e202200645
[51] Abdul Kareem T and Anu Kaliani A 2012 Glow discharge plasma electrolysis for nanoparticles synthesis *Ionics* **18** 315–27
[52] Saito G and Akiyama T 2015 Nanomaterial synthesis using plasma generation in liquid *J. Nanomater.* **2015** 123696
[53] Wüthrich R, Comninellis C and Bleuler H 2005 Bubble evolution on vertical electrodes under extreme current densities *Electrochim. Acta* **50** 5242–6
[54] Lu X, Mohedano M, Blawert C, Matykina E, Arrabal R, Kainer K U and Zheludkevich M L 2016 Plasma electrolytic oxidation coatings with particle additions—a review *Surf. Coat. Technol.* **307** 1165–82
[55] Li G, Ma F, Liu P, Qi S, Li W, Zhang K and Chen X 2023 Review of micro-arc oxidation of titanium alloys: mechanism, properties and applications *J. Alloys Compd.* **948** 169773
[56] Fascio V, Wüthrich R and Bleuler H 2004 Spark assisted chemical engraving in the light of electrochemistry *Electrochim. Acta* **49** 3997—4003
[57] Wüthrich R and Abou Ziki J D 2015 *Micromachining Using Electrochemical Discharge Phenomenon* (Waltham)
[58] Schaper L, Graham W G and Stalder K R 2011 Vapour layer formation by electrical discharges through electrically conducting liquids-modelling and experiment *Plasma Sources Sci. Technol.* **20** 034003
[59] Schaper L, Stalder K R and Graham W G 2011 Plasma production in electrically conducting liquids *Plasma Sources Sci. Technol.* **20** 034004
[60] Forschner L, Gembus J-L, Schücke L, Awakowicz P, Gibson A R, Jacob T and Engstfeld A K 2025 Statistical analysis of the dynamic behavior of individual discharges during the ignition and continuous phases of contact glow discharge electrolysis *J. Phys. D: Appl. Phys.* **58** 215204
[61] Raizer Y P 1991 *Gas Discharge Physics* (Springer)
[62] Fridman A 2008 *Plasma Chemistry* (Cambridge University Press)
[63] Lieberman M A and Lichtenberg A J 2005 *Plasma Chemistry* (Wiley)
[64] Saifutdinov A I 2022 Numerical study of various scenarios for the formation of atmospheric pressure DC discharge characteristics in argon: from glow to arc discharge *Plasma Source Sci. Technol.* **31** 094008
[65] Druyvesteyn M J and Penning F M 1940 The mechanism of electrical discharges in gases of low pressure *Rev. Mod. Phys.* **12** 87–174
[66] Hermanns P, Kogelheide F, Bracht V, Ries S, Krüger F, Böddeker S, Bibinov N and Awakowicz P 2021 Formation and behaviour of plasma spots on the surface of titanium film *J. Phys. D: Appl. Phys.* **54** 085203
[67] Saifutdinov A I 2021 Unified simulation of different modes in atmospheric pressure DC discharges in nitrogen *J. Appl. Phys.* **129** 093302
[68] Anders A 2024 Glows, arcs, ohmic discharges: an electrode-centered review on discharge modes and the transitions between them *Appl. Phys. Rev.* **11** 031310
[69] Baeva M and Uhrland D 2025 Characterization and applications of direct current microarcs: a review *J. Phys. D: Appl. Phys.* **58** 263001
[70] Zhang J, Yuan H, Zhou Z, Liang R, Lu K, Li S and Yang D 2025 Plasma characteristics and mode transitions of needle-to-needle discharge in ambient air *J. Phys. D: Appl. Phys.* **58** 205202
[71] Jovanović A P, Höft H, Loffhagen D, Becker M M and Gerling T 2025 Discharge modes of self-pulsing discharges in argon at atmospheric pressure *J. Phys. D: Appl. Phys.* **58** 275204
[72] Bazelyan E M and Raizer Y P 1998 *Spark Discharge* (Taylor & Francis)
[73] Scheeline A, Kamla G J and Zoellner M J 1984 Electron concentration measurement in the high voltage spark using Stark broadening of H, emission *Spectrochim. Acta* **39B** 677–91

[74] Sankhé M, Bernard S, Wartel M, Pellerin S and Gillard P 2019 Characterization of a spark discharge for dust cloud ignition *Contrib. Plasma Phys.* **59** 326–39
[75] Forschner L, Artmann E, Jacob T and Engstfeld A K 2023 Electric potential distribution inside the electrolyte during high voltage electrolysis *J. Phys. Chem. C* **127** 4387–94
[76] Nikiforov A Y, Leys C, Gonzales M A and Walsh J L 2015 Electron density measurement in atmospheric pressure plasma jets: stark broadening of hydrogenated and non-hydrogenated lines *Plasma Sources Sci. Technol.* **24** 034001
[77] Laux C O, Spencer T G, Kruger C H and Zare R N 2003 Optical diagnostics of atmospheric pressure air plasmas *Plasma Sources Sci. Technol.* **12** 125–38
[78] Bruggeman P, Schram D, Gonzales M A, Rego R, Kong M G and Leys C 2009 Characterization of a direct dc-excited discharge in water by optical emission spectroscopy *Plasma Sources Sci. Technol.* **18** 025017
[79] Bruggeman P, Schram D C, Kong M G and Leys C 2009 Is the rotational temperature of OH(A–X) for Discharges in and in contact with liquids a good diagnostic for determining the gas temperature? *Plasma Process. Polym.* **6** 751–62
[80] Abila P A and Trassy C 1989 Rotational temperatures and LTE in argon ICP *Microchim. Acta* **99** 159–68
[81] Ishii I and Montaser A 1991 A tutorial discussion on measurements of rotational temperature in inductively coupled plasmas *Spectrochim. Acta* **46** 1197–206
[82] Richardson O W 1914 The distribution of the molecules of a gas in a field of force, with applications to the theory of electrons *Lond. Edinb. Dubl. Phil. Mag.* **28** 633–47
[83] Dushman S 1930 Thermionic emission *Rev. Mod. Phys.* **2** 381–476
[84] Jensen K L 2024 Tutorial: the equations of electron emission and their evaluation *J. Appl. Phys.* **135** 11101
[85] Huber E E 1966 The effect of mercury contamination on the work function of gold *Appl. Phys. Lett.* **8** 169–71
[86] Kasper C 1940 the theory of the potential and the technical practice of electrodeposition: I. the general problem and the cases of uniform flow *Trans. Electrochem. Soc.* **77** 353–63
[87] Asimakoulas L, Graham W G, Krcma F, Dostal L, Stalder K R and Field T A 2020 Fast framing imaging and modelling of vapour formation and discharge initiation in electrolyte solutions *Plasma Sources Sci. Technol.* **29** 035013
[88] Gilliam R J, Graydon J W, Kirk D W and Thorpe S J 2007 Review of specific conductivities of potassium hydroxide solutions for various concentrations and temperatures *Int. J. Hydrog. Energy* **32** 359–64
[89] Staack D, Farouk B, Gutsol A and Fridman A 2008 DC normal glow discharges in atmospheric pressure atomic and molecular gases *Plasma Sources Sci. Technol.* **17** 025013